frontiers | Frontiers in Chemical Engineering

TYPE Original Research
PUBLISHED 15 May 2023
DOI 10.3389/fceng.2023.1160254

OPEN ACCESS

EDITED BY
Wen Luo,
Shanghai University, China

REVIEWED BY
Lole Jurado,
Institut Català d'Investigació Química, Spain
Jingjie Luo,
Dalian University of Technology, China

*CORRESPONDENCE
Liping Zhong,
liping.zhong@epfl.ch

SPECIALTY SECTION
This article was submitted to Catalytic Engineering, a section of the journal Frontiers in Chemical Engineering

RECEIVED 06 February 2023
ACCEPTED 20 March 2023
PUBLISHED 15 May 2023

CITATION
Zhong L, Pham THM, Ko Y and Züttel A (2023), Graphene nanoplatelets promoted CoO-based catalyst for low temperature CO_2 methanation reaction. *Front. Chem. Eng.* 5:1160254. doi: 10.3389/fceng.2023.1160254

Graphene nanoplatelets promoted CoO-based catalyst for low temperature CO_2 methanation reaction

Liping Zhong[1,2]*, Thi Ha My Pham[1,2], Youngdon Ko[1,2] and Andreas Züttel[1,2]

[1]Laboratory of Materials for Renewable Energy (LMER), Basic Science Faculty (SB), Institute of Chemical Sciences and Engineering (ISIC), École Polytechnique Fédérale de Lausanne (EPFL) Valais/Wallis, Sion, Switzerland, [2]Empa Materials Science and Technology, Dübendorf, Switzerland

Methanation of CO_2 is an important reaction for reducing CO_2 emissions in a power-to-gas system. Compared to cobalt supported on gamma-Al_2O_3, cobalt supported on graphene nanoplatelets (GNPs) showed significantly better performance for CO_2 methanation. Cobalt supported on GNPs was capable of 15% conversion of CO_2 to CH_4 at temperatures below 250°C, compared to 5% for cobalt supported on Al_2O_3. *In situ* thermogravimetric analysis (TGA) demonstrated that the Co/GNP catalyst was stable to 400°C. The maximum catalyst mass-specific CH_4 yield was obtained at a Co loading of 5_{wt}% on GNPs; however, high Co loading on GNPs deactivated the reactivity of the Co/GNP catalyst. Transmission electron microscopy (TEM) demonstrated that 5_{wt}% Co/GNPs had the smallest and most dispersed cobalt nanoparticles. Excessive loading of cobalt tended to form isolated large Co nanoparticles. X-ray photoelectron spectroscopy (XPS) and Raman spectrometry revealed that more CoO phases were maintained on the surface of 5_{wt}% Co/GNPs, indicating that the interaction between the Co and the GNPs had more of an impact on cobalt's redox capacity than did particle size, which ultimately affected cobalt's active phase during the CO_2 reduction process. Furthermore, Raman spectrometry demonstrated that Co loading led to an increase in graphene defects. Higher Co loading on GNPs resulted in fewer interfaces between Co and GNPs due to the agglomeration of Co nanoparticles.

KEYWORDS

CO_2 reduction, CoO catalyst, graphene support, methanation, metal–support interaction

1 Introduction

Researchers agree that global warming is mostly caused by CO_2 emissions from excessive use of fossil fuels (Johnsson et al., 2019). Over the decades, processes for CO_2 reduction have been extensively studied and tested but with little real progress. For example, CO_2 can be converted into other chemicals, such as CH_4, CH_3OH, and CH_3COOH, *via* various techniques such as thermal, electrochemical, photochemical, biochemical, and plasmatic techniques (Jimenez et al., 2011; Mateo et al., 2018; Ojelade and Zaman, 2021; Pham et al., 2022). Among these, the thermal catalytic methanation process, also known as the Sabatier reaction, has been considered the most competitive CO_2 reduction process for commercial application due to the high energy yield and conversion efficiency. In a power-to-gas system,

CH_4 produced from CO_2 can be directly fed into the power plant for producing electricity, reducing the demand for natural gas (Bailera et al., 2017). Commercialization of the CO_2 methanation process benefits society not only through the reduction of CO_2 but also the replacement of fossil fuel by a renewable energy resource (Bacariza et al., 2020). However, the efficiency of the CO_2 methanation process is critically dependent on the activity of the catalyst.

The CO_2 conversion rate and CH_4 yield are limited by the thermodynamic equilibrium of CO_2 methanation at high temperatures; an ideal catalyst should be selective and function at relatively low temperatures (Kuśmierz, 2008; Wang et al., 2016). The transition metals Ru, Rh, Co, and Ni, supported on porous materials such as Al_2O_3, CeO_2, and TiO_2, have been reported to be active for CO_2 methanation (Frontera et al., 2017). The noble metal ruthenium- and rhenium-based catalysts have shown excellent activity and selectivity over a wide temperature range, but their high market price has stimulated the development of cobalt and nickel catalysts as replacements. Ni/CeO_2 has been shown to be comparable to the noble metal catalysts, but only at elevated temperatures, where it tends to be deactivated because of the agglomeration of Ni particles and coking on the catalyst's surface (Vogt et al., 2018). In contrast, cobalt-based catalysts have demonstrated better reactivity at low temperatures (Ci et al., 2010; Liu et al., 2018; Parastaev et al., 2020; Tu et al., 2021). The active structure of cobalt-based catalysts has been determined to be the CoO phase (ten Have et al., 2022), (Zhao et al., 2020). However, this transition phase tends to be reduced to metallic Co by the reductive mixture of CO_2 and H_2, leading to studies on stabilizing the active phase for long-term reactivity (Zhong et al., 2019; Zhong et al., 2021a; Zhong et al., 2021b).

In order to maintain the stability of the catalytic CoO phase during the CO_2 methanation reaction, it is essential to tune the redox ability of Co. Conventionally, the redox ability of Co can be adjusted by changing particle size, interaction with the support, or with a second promoter (Wigzell and Jackson, 2017; Qi et al., 2020; Rahmati et al., 2020). As reported previously, the insertion of a graphene layer into a Co/ZnO system results in a more reductive surface in an oxidative environment. Graphene is also able to tune Co particles (He et al., 2013; Karimi et al., 2015; Cañón and Teplyakov, 2021). Inspired by those results, we used graphene nanoplatelets as supports for cobalt-based CO_2 methanation catalysts. Bulk and surface characterization methods were used to investigate the promotion mechanism of the GNP support. To the best of our knowledge, this is the first time that a carbonaceous material like GNP, has been used as a catalyst support for the thermal CO_2 reduction process.

2 Experimental methods

2.1 Materials and catalyst preparation

The Co-based catalysts were prepared by the incipient impregnation wetness method. For the Co/Al_2O_3 sample, $Co(NO)_3{\cdot}6H_2O$ (Alfa Aesar, CAS#10026-22-9) was dissolved in deionized water (DIW). Al_2O_3 (2 g) was impregnated into the cobalt nitrate solution, and the mixture was dried at 80°C in air. For the Co/GNP samples, the cobalt nitrate was dissolved in a mixture of DIW and ethanol (1:1, vol%) because of the hydrophobic nature of the GNP (Sigma-Aldrich, CAS#7782-42-5) surface. The solution was then applied to the GNPs based on the saturated water absorption of the support, and this was repeated three times. For the gamma Al_2O_3 support (Jiangxi, Pingxiang, Alibaba.com), the cobalt nitrate was dissolved in DIW and the solution was impregnated three times. After the impregnation step, the samples were dried in air at 80°C for around 12 h. After drying, the as-prepared sample was directly loaded into a fixed-bed reactor. Before starting the CO_2 methanation, *in-situ* reduction of the sample with 5% H_2 (by vol) at 400°C for 2 h was performed to anneal the Co precursor to the metallic Co. For characterizations, the samples were reduced in 5% H_2 (by vol) balanced with N_2 at 400°C for 2 h, and then collected for different measurements.

2.2 Material characterization

The Brunauer–Emmett–Teller (BET) surface area of the supports was obtained by the N_2 adsorption–desorption method using a BELSORP MAX II analyzer from Microtract MRB. The loading content of Co in each sample was determined with an Agilent 5110 inductively coupled plasma optical emission spectrometer (ICP-OES). X-ray diffraction patterns were obtained on a Bruker D8 Advance instrument (40 kV, 40 mA, Cu Kα radiation, and λ = 0.154 nm). X-ray photoelectron spectroscopy (XPS) and Raman spectroscopy were used for surface characterization. The XPS spectra of Co 2p were collected under ultra-high-vacuum (UHV) on a Kratos Axis Supra XPS system using the monochromatic Kα line of an aluminum X-ray source (1486.6 eV) with the analyzer set at a pass energy of 20 eV. The deconvolution of the Al 2p peak was completed with CasaXPS software. Raman spectroscopy was obtained under ambient conditions using a 632-nm laser. Scanning electron microscopy (SEM) images were acquired on a Thermo-Fisher Teneo FE-SEM. Transmission electron microscopy images were acquired with Thermo-Fisher Tecnai Osiris (200 kV) and Thermo-Fisher Tecnai Spirit (120 kV) EMs. Thermo-gravimetric analysis (TGA) was performed using a TG 209 F1 Libra instrument by Netzsch.

2.3 Catalytic activity evaluation

The reactivity of catalysts for CO_2 methanation was evaluated in a microscale fixed-bed flow reactor. The reactor consists of a 5-cm-long stainless steel tube with an inner diameter of 8 mm for the catalyst bed zone and a temperature control system. The catalyst sample was loaded as pellets with a size of 40–60 mesh. The catalyst bed zone was heated in a furnace with the reaction temperature measured by a K-type thermocouple running through the catalyst bed. For each test, 200 mg of sample pellets were loaded into the reactor and reduced with 10% (by vol) H_2 (2 ml/min H_2 + 8 ml/min N_2) at 400°C for 3 h. After the temperature had cooled to 50°C, the gas mixture was switched to 3 ml/min of CO_2, 4.5 ml/min of N_2, and 12 ml/min of H_2. For each reaction at a specific temperature, a dwell of 2 h was set, after which the outlet gas was analyzed on a gas chromatograph (SRI 83670) with a thermal conductivity detector

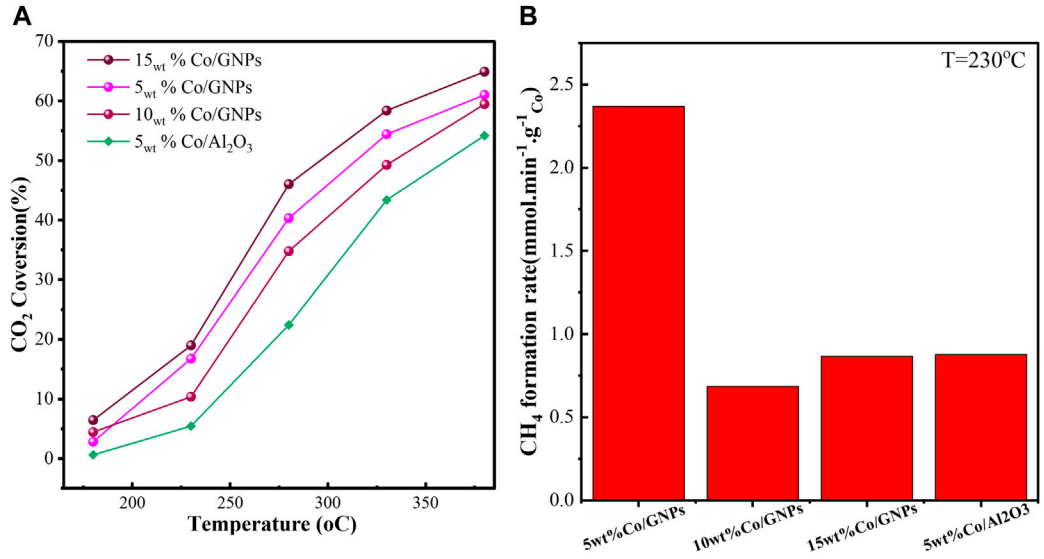

FIGURE 1
CO_2 conversion of catalysts at different temperatures **(A)** and the mass-specific CH_4 formation rate of cobalt in each catalyst at 230°C **(B)**. Reaction conditions: 1 bar, 19.5 ml/min total flow rate with reaction mixtures of 15_{vol}% of CO_2, 60_{vol}% of H_2, and 25_{vol}% of N_2.

(TCD). The CO_2 conversion (X_{CO2}), CO selectivity (S_{CO}), and CH_4 selectivity (S_{CH4}) rate were determined separately by Eqs 1–3:

$$X_{CO2} = \frac{CO_{2,in} - CO_{2,out}}{CO_{2,in}}, \quad (1)$$

$$S_{CO} = \frac{CO_{out}}{CO_{2,in} - CO_{2,out}}, \quad (2)$$

$$S_{CH4} = \frac{CH_{4,out}}{CO_{2,in} - CO_{2,out}}, \quad (3)$$

where CO_2, $_{out/in}$, CH_4 $_{out}$, and CO_{out} are the molar concentrations of the reactor inlet/outlet gas stream. For each gas, the molar concentration was determined by external calibration curves with standard gases. For correction of the total volume change from inlet to outlet due to the reaction, N_2 was used as an internal standard calibration gas. In order to compare the intrinsic activity of Co in each sample, we have calculated the Co mass-specific CH_4 formation rate by Eq. (4):

$$R_{CH4} = \frac{X_{CO2} \times S_{CH4} \times F_{CO2,in}}{V_m \times Co_{wt}\% \times m_{catalyst}}, \quad (4)$$

where $\mathbf{V_m}$ is the molar volume of ideal gas at standard conditions, which is 22.4 L/mol, while $\mathbf{m_{catalyst}}$ is the mass of the catalyst loaded for each test. Co% is the cobalt content in weight percentage, as defined by ICP-OES analysis.

3 Results and discussion

3.1 Catalytic reactivity

The reactivity of supported Co catalysts for the hydrogenation of CO_2 to methane is shown in Figure 1. For the same Co loading (5_{wt}%), Co supported on GNPs exhibited a much higher CO_2 conversion rate than on Al_2O_3. For example, only 5% CO_2 conversion is obtained with 5_{wt}% Co/Al_2O_3 at 235°C, while the conversion rate is 15% for 5_{wt}% Co/GNPs. Unexpectedly, the increased Co loading on GNPs did not equate to a comparable rise in CO_2 conversion. Much less CO_2 was converted by 10_{wt}% Co/GNPs than by 5_{wt}% Co/GNPs. Figure 1B also compares the Co mass-specific CH_4 production of four catalysts at kinetic-dominated temperatures to directly assess the intrinsic reactivity of Co in each sample. The Co mass-specific yield of CH_4 of 10_{wt}% Co/GNPs was lower than that of 5_{wt}% Co/Al_2O_3. The results clearly indicate that a catalyst with 5_{wt}% Co supported on GNPs was the most reactive, while the 10_{wt}% Co loaded on GNPs had the lowest reactivity. The difference in mass-specific reactivity can likely be attributed to the different active phases of Co in each sample. The characteristics of this Co phase are revealed in the following results and analysis.

3.2 Bulk and morphology properties

To investigate the intrinsic effects of GNPs on Co catalysis for CO_2 conversion, we tested commercial GNPs and compared them to porous Al_2O_3 supports with the same surface area (300 m^2/g) as a reference. The BET surface area was determined, and results can be found in supporting information (Supplementary Table S1; Supplementary Figure S1). The porous Al_2O_3 material is commonly used as a support in commercial and industrial-scale operations for fabricating supported-metal catalysts because of its relatively low price and compatibility with different application conditions. Even though other reducible oxides, like CeO_2, ZrO_2, and ZnO, have been reported as promising supports for cobalt-based CO_2 methanation, the intrinsic reactivity of those oxides for CO_2

TABLE 1 ICP-OES quantification results of cobalt content in reduced catalyst samples.

Sample	Nominal mass content Co/(Co + support)%	ICP-OES analyzed result (wt%)
5_{wt}%Co/Al_2O_3	5.00	4.17
5_{wt}%Co/GNPs	5.00	4.74
10_{wt}%Co/GNPs	10.00	10.15
15_{wt}%Co/GNPs	15.00	14.69

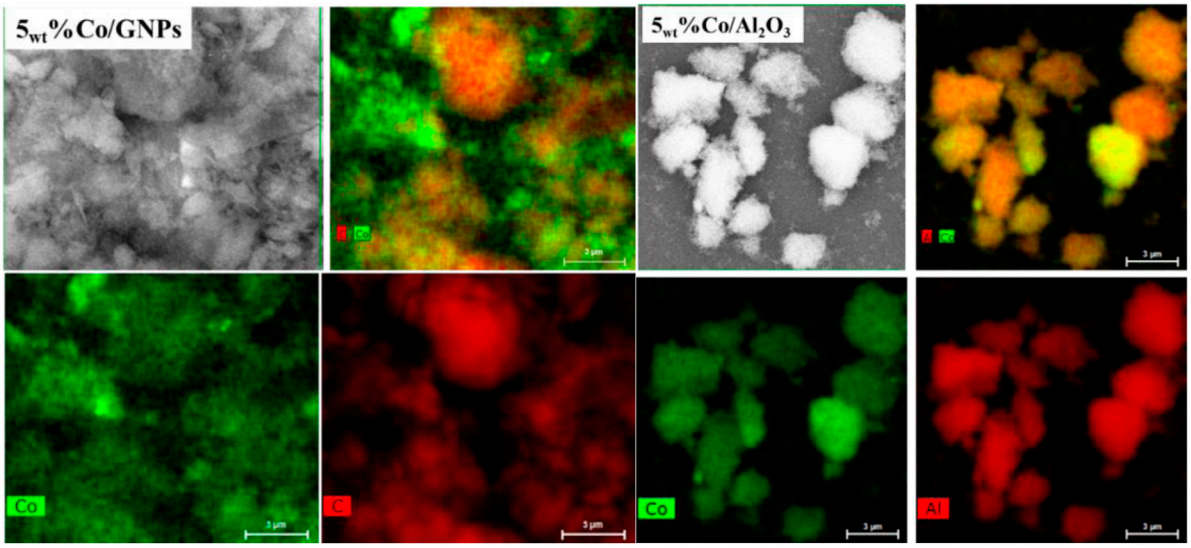

FIGURE 2
Representative SEM-EDX mapping images of cobalt supported on GNPs (*left*) and Al_2O_3 (*right*) after reduction by H_2.

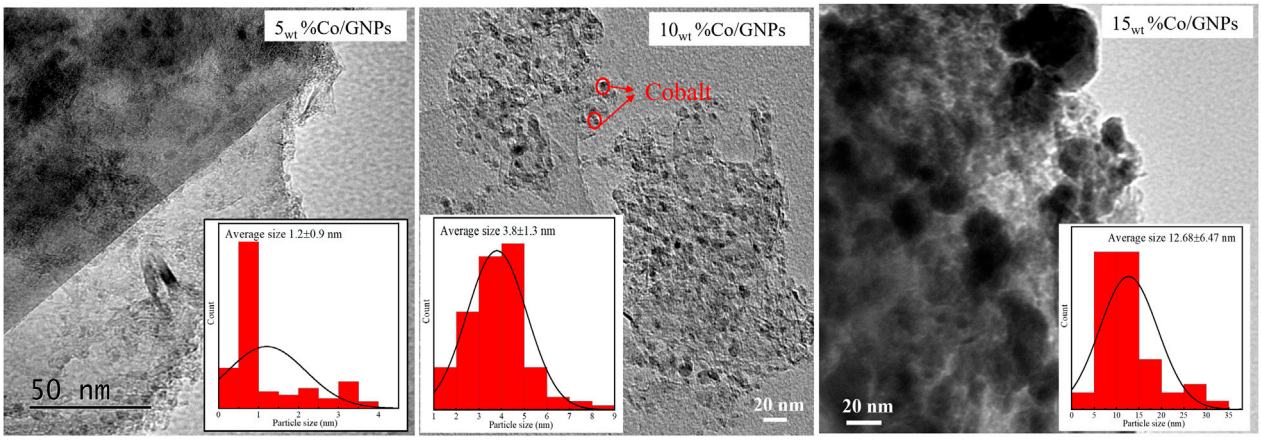

FIGURE 3
TEM images and cobalt particle size distribution of Co/GNP samples after reduction at 400°C by H_2.

conversion complicates the determination of the specific influences of the cobalt–support interaction. In this study, the selected pure Al_2O_3 and GNPs are both inert in the CO_2 methanation reaction at the tested temperatures. The Co content in the tested catalysts was confirmed by IPC-OES, and all the catalysts had the designated Co content (Table 1). The small discrepancies between nominal content

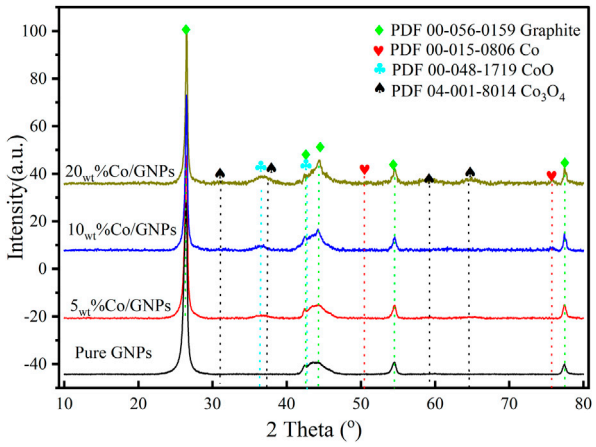

FIGURE 4
Full XRD patterns of GNP-based samples. Samples were first reduced with H_2 at 400°C and measured *ex situ* in air.

and content in synthesized samples were probably due to deviations occurring during synthesis.

SEM-EDX mapping results (Figure 2) demonstrate that the 5_{wt}% of Co applied is distributed uniformly onto both Al_2O_3 and GNP supports. Only a few regions in the map show a heavier Co deposit, indicating that most Co clusters were resistant to agglomeration during reduction at 400°C. TEM images (Figure 3) of Co/GNP samples show that increasing Co loading to 15_{wt}% leads to formation of large Co aggregates. Cobalt particles of about 1 nm are formed and are well dispersed in the 5_{wt}% Co/GNP sample, but their average size rose to 3.8 nm in the 10wt% Co/GNP sample. Large cobalt particles up to 30 nm were formed when Co content was increased to 15_{wt}%. Large particles typically have a relatively low surface area, which results in fewer sites for reaction. This may help explain why larger loading results in a lower metal-mass-specific yield of CH_4. Although the sample with 10_{wt}% loading had smaller cobalt particles than that with 15_{wt}% loading, which is believed to have a higher active surface area of Co, it exhibited lower CH_4 yield than the 15_{wt}% catalyst. The discrepancy between the Co surface area and reactivity may be explained by the finding, which is supported by numerous studies, that the catalytic reactivity of Co is dependent on its particle size. In those investigations, it was discovered that the size of Co affects its redox capacity and defines the active phase during reaction (Ci et al., 2010; Sadasivan et al., 2013; Torshizi et al., 2021).

Figure 4 shows the crystalline structure of Co and GNPs. A wide peak around $2\theta = 36°$ is attributed to the CoO (220) crystalline phase (PDF#00-048-1719) in all Co/GNP samples. The Co_3O_4 phase (PDF#04-001-8014) was only detected in the 15_{wt}% Co/GNPs, while the metallic Co crystalline phase was found in both the 10_{wt}% Co/GNPs and 15_{wt}% Co/GNPs. Although all samples were reduced under the same conditions, they were oxidized during the *ex situ* measurement and transition due to exposure to air. The differences in the crystalline phase of Co in the three samples indicate that its redox ability might be different, suggesting some mechanistic aspects of the different Co active sites. This redox ability is dependent on Co particle size and interactions between Co and the GNP support (Sadasivan et al., 2013). It has been reported that smaller Co metal particles were oxidized more readily than bigger particles. According to TEM size analysis, the 5_{wt}% Co catalyst had the smallest particle size. Although it was oxidized under the same conditions, the XRD pattern showed no Co_3O_4 phase in this sample. In addition to particle size, the interaction between the Co and the support plays a key role in determining its redox activity. We hypothesized that the metal–support interaction plays an essential role in Co's redox ability, eventually affecting the Co active phase for CO_2 methanation.

3.3 Surface properties

Structural analysis of Co catalysts has revealed that the size of Co particles was dominated by the Co loading content. The size of the Co particles has always been considered a key aspect in the reactivity of Co, but the variation in reactivity with particle size did not agree with the findings in our study. Co's crystalline phase also varies with the loading content, demonstrating that Co's active phase in Co/GNPs catalysts might be different. To further define the active phase of Co, XPS and Raman spectrometry, which are powerful surface-sensitive techniques, have been used for verifying the surface phase of catalysts. In Figure 5, two satellite peaks at 785.8eV and 789.8eV indicate the coexistence of CoO (referred to as Co^{2+}) and Co_3O_4 (referred to as Co^{3+}) phases, respectively; meanwhile, the peak of metallic Co (about 778 eV) was not observed (Khassin, 2001; Lahijani et al., 2015; Cañón and Teplyakov, 2021). The deconvolution of the Co 2p peak based on previous literature studies allowed calculation of the ratio of Co^{2+}/Co^{3+} on the surface. As summarized in Table 2, the ratio of Co^{2+}/Co^{3+} of the tested catalysts followed the trend of 5_{wt}%Co/GNPs > 5_{wt}%Co/Al_2O_3 > 15_{wt}%Co/GNPs >10_{wt}%Co/GNPs, which is consistent with the trend of their intrinsic Co activity (Figure 1B). This trend indicates that CoO is the preferred phase for CO_2 conversion, as reported. The different amounts of CoO formed on the catalyst's surface were related to the redox ability of Co which is normally related to Co particle size and metal–support interactions (Torshizi et al., 2021; Díez-Ramírez et al., 2017; Parastaev et al., 2020). The GNP support was more conducive to the formation of the CoO phase for the reaction compared to the influence of particle size.

Figure 6A shows the typical Raman spectra of GNPs in catalysts and as a support only. A strong G-band peak appears at about 1583 cm^{-1} attributed to the E_{2g} mode, which is caused by stretching of the C-C bond in all carbon materials. A 2D band peak located around 2700 cm^{-1} confirms the graphitic structure of GNPs. (Ci et al., 2010), (Luo et al., 2017) The relative low intensity of the 2D band together with a red shift location indicates that GNPs contain multiple graphene layers. Another peak at about 1350 cm^{-1} is the signature of the D band caused by disorder in the graphene structure. It is known that doping with transition metals, Ni, Co or Pt, leads to extrinsic disorder in graphene structure with formation of covalent bonds between C-atoms (Krasheninnikov et al., 2009; Xin et al., 2016). The quantification of the relative ratio between the intensities of the D band and the G band (I_D/I_G) provides information on the degree of disorder in the graphene layers after Co loading (Cançado et al., 2011) (Table 2). The 5_{wt}% Co/GNPs catalyst has the highest I_D/I_G ratio at 0.17, while the

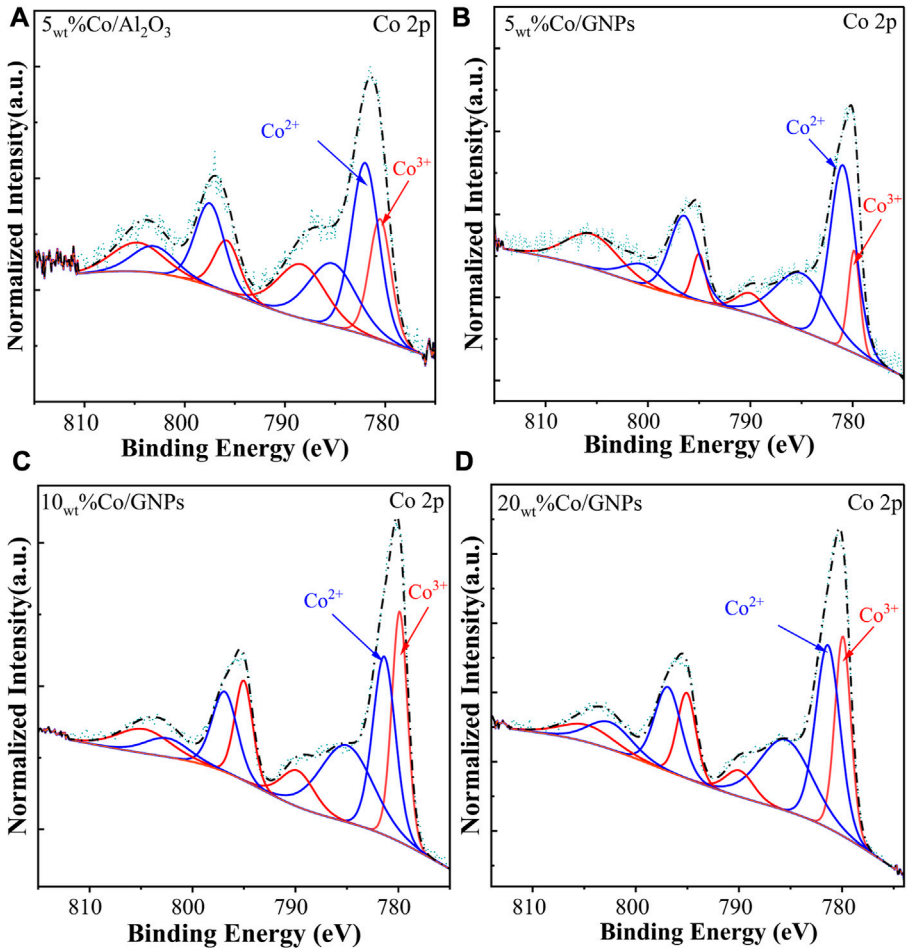

FIGURE 5
High-resolution XPS spectra of Co 2p for cobalt-based catalysts. All samples were reduced at 400°C with 5% H_2 in N_2 before measurement.

TABLE 2 Ratio of different cobalt species and the graphene phase on the surface of the catalyst and support analyzed by XPS and Raman spectrometry, respectively.

Sample	Co^{2+}/Co^{3+} acquired by XPS results	I_D/I_G acquired by Raman results
5_{wt}%Co/ɤ-Al_2O_3	1.81	-
5_{wt}%Co/GNPs	5.03	0.17
10_{wt}%Co/GNPs	1.12	0.15
15_{wt}%Co/GNPs	1.41	0.15
Pure GNPs	-	0.10

support alone has the lowest I_D/I_G ratio at 0.10. However, loading more Co does not increase the disorder but results in less disorder. According to theoretical calculations (Krasheninnikov et al., 2009), the addition of a dopant to graphene shifts the Fermi-level of carbon, leading to the enhancement of conductivity and catalytic activity. This helps explain why the 5_{wt}% Co/GNP sample had the highest reactivity for CO_2 conversion. In this sample, it is also possible that more Co interacted with graphene, leading to a more stable electronic structure resisting the redox transformation of the CoO phase under reaction conditions. The agglomeration of Co clusters results in lower formation of interfaces or boundaries between graphene and Co.

The Raman spectra of the Co phase are shown in Figure 6B. Five intense peaks located at 191, 470, 515, 608, and 675 cm^{-1} were found in all the Co/GNP samples. Based on previous results, a CoO octahedron-shaped sample registers three Raman peaks around

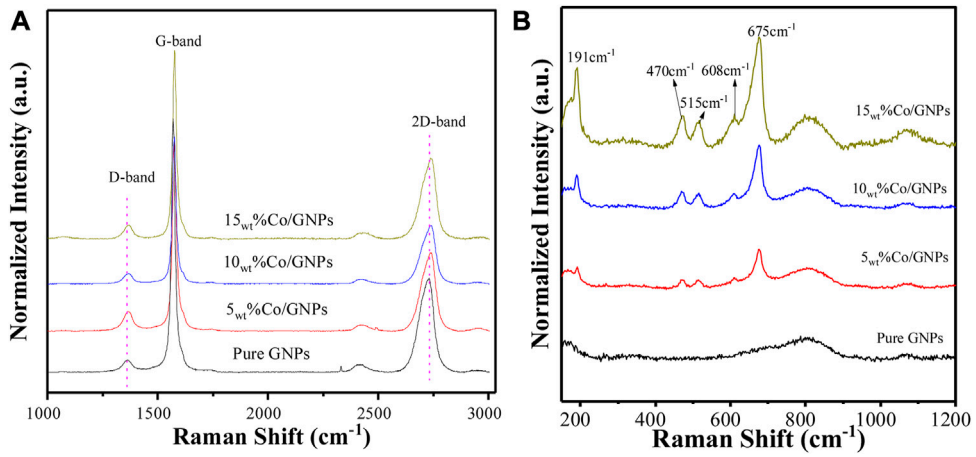

FIGURE 6
Raman spectra of catalysts and pure GNPs; the range of carbon features is shown in **(A)**, while the cobalt features are depicted in **(B)**. The Co/GNP samples were reduced before measurement, while the pure GNPs were measured directly without any pretreatment.

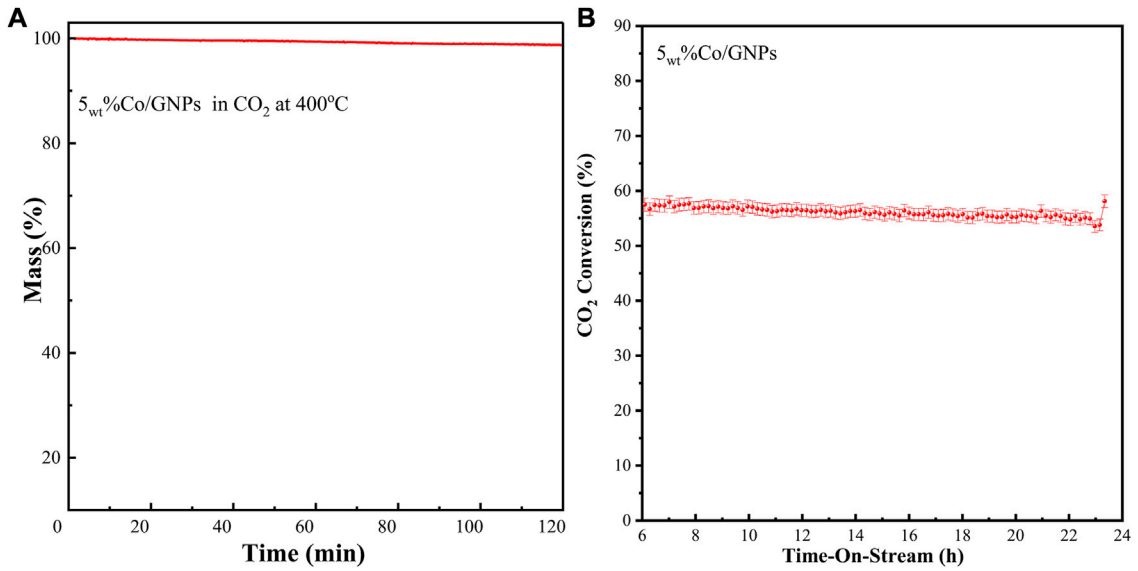

FIGURE 7
(A) TGA curve of the 5wt% Co/GNP sample after reduction in a continuous CO_2 stream; **(B)** time-on-stream of CO_2 conversion by a 5_{wt}% Co/GNPs catalyst tested at 350°C under constant reaction conditions: 1 bar, 19.5 ml/min total flow rate with a reaction mixture containing 15_{vol}% of CO_2, 60_{vol}% of H_2, and 25_{vol}% of N_2.

515 cm^{-1}, 555 cm^{-1}, and 680 cm^{-1} (Ravindra et al., 2014), while Co_3O_4 with a spinel structure has five Raman-active modes: A1g, Eg, and three T2g modes located around 194 cm^{-1}, 479 cm^{-1}, 515 cm^{-1}, 617 cm^{-1}, and 686 cm^{-1}, respectively. Among the five modes, the A1g mode at 194cm-1 is the most intense (Hadjiev et al., 1988). For the stretching of Co-O, the nanoscale size of the sample and distortions of the lattice due to defects leads to the shift of position and change in intensity (Li et al., 2016). These characteristic peaks were observed in all samples with slight shifts, indicating the co-existence of CoO and Co_3O_4 oxide on the sample surface. This agrees with the XPS results, which always depict a face with a mixture of Co^{3+} and Co^{2+}. It should be noted that the applied laser could also cause CoO oxidation, resulting in more Co_3O_4 phase, which complicates the discussion [44]. However, the relative ratio of Co_3O_4 in the sample can be derived indirectly from the intensity of the peak at 191cm-1 that corresponds to the A1g mode of the Co_3O_4 phase. The spectra demonstrate that 5_{wt}% Co/GNP has the weakest peak at 191cm-1 after normalization, indicating that this catalyst has the highest CoO ratio, but the smallest amount of the Co_3O_4 phase. This finding is

consistent with the XPS results, highlighting the CoO phase's established reactivity for CO_2 methanation.

3.4 Stability

The stability of carbon materials is always a concern for application in thermal CO_2 conversion reactions due to the reverse Boudouard reaction of $CO_2 + C - 2CO$ (Lahijani et al., 2015). This reaction, also known as the CO_2 gasification reaction, is thermodynamically supported at temperatures above 350°C, and at ambient pressure. In the case of a GNP-supported catalytic system for CO_2 methanation, if the GNPs interact with the CO_2 reactants, the support lifetime will be limited. Herein, we have used CO_2-TGA to determine the stability of a synthesized GNP-supported Co catalyst. The test was performed at higher temperatures than the ideal CO_2 methanation temperature of 200–300°C. Figure 7A demonstrates that the sample mass remains steady in CO_2 at 400°C up to 2 h. The time-on-stream CO_2 conversion of this catalyst running at 350°C shows a lifetime up to 24 h with only a slight decrease. This decrease is perhaps caused by the agglomeration of cobalt particles, as indicated in TEM images (Figure 3); stabilization of the Co particles should obviate this problem.

4 Conclusions

Commercial GNP material was used as a support of a cobalt catalyst for CO_2 methanation. The as-synthesized Co/GNP catalysts exhibited higher intrinsic reactivity than the Al_2O_3-supported Co catalyst. The best Co/GNPs, according to the reactivity tests, were obtained with a loading of 5_{wt}% Co. TEM size analysis showed that larger Co particles were formed with increased Co loading, while Raman spectra showed that the growth of cobalt nanoparticles reduced the formation of interfaces between Co and the graphene surface, ultimately influencing the total number of Co active sites. As a result, fewer surface defects of graphene were produced in high-loading (10_{wt}% and 15_{wt}%) Co/GNP samples, which corresponded to lower catalytic reactivity and CH_4 yield. Cobalt surface analysis using XPS and Raman spectra showed that a higher oxidative phase of Co (Co^{3+}) was observed on the surface of materials with high Co loading. With the same loading, the sample supported by GNPs had more of the Co^{2+} phase than the cobalt supported by Al_2O_3. Accordingly, we conclude that the GNP support promotes the formation and maintenance of more of the reactive Co^{2+} phase on the catalyst surface for CO_2 methanation. Modest Co loading (5_{wt}%) promoted the formation of graphene defects while simultaneously forming more CoO active phases for increased reactivity. In conclusion, this research has been the first to demonstrate the potential reactivity of a carbon-supported Co catalyst and the synergistic role of graphene support for CO_2 thermal methanation. Further efforts need to be devoted to improving the lifetime of this catalyst system.

Data availability statement

The original contributions presented in the study are included in the article/Supplementary Material. Further inquiries can be directed to the corresponding author.

Author contributions

LZ performed the synthesis, tests, characterization, data analysis, and paper drafting. TM performed the TEM and SEM microscopy measurements. YK measured the TGA and ICP-OES catalysts. LZ wrote the paper, with inputs from other authors. AZ reviewed the paper. All authors contributed to the article and approved the submitted version.

Funding

This research was supported by GAZNAT and the Swiss Federal Office of Energy (SFOE) under contract SI/502228-0.

Acknowledgments

The authors acknowledge the financial support of EPFL and Empa in Switzerland.

Conflict of interest

The authors declare that the research was conducted in the absence of any commercial or financial relationships that could be construed as a potential conflict of interest.

Publisher's note

Supplementary material

The Supplementary Material for this article can be found online at: https://www.frontiersin.org/articles/10.3389/fceng.2023.1160254/full#supplementary-material

References

Bacariza, M. C., Spataru, D., Karam, L., Lopes, J. M., and Henriques, C. (2020). Promising catalytic systems for CO2 hydrogenation into CH4: A review of recent studies. *Processes* 8 (12), 1–45. doi:10.3390/pr8121646

Bailera, M., Lisbona, P., Romeo, L. M., and Espatolero, S. (2017). Power to Gas projects review: Lab, pilot and demo plants for storing renewable energy and CO2. *Renew. Sustain. Energy Rev.* 69, 292–312. doi:10.1016/J.RSER.2016.11.130

Cançado, L. G., Jorio, A., Ferreira, E. H. M., Stavale, F., Achete, C. A., Capaz, R. B., et al. (2011). Quantifying defects in graphene via Raman spectroscopy at different excitation energies. *Nano Lett.* 11 (8), 3190–3196. doi:10.1021/nl201432g

Cañón, J., and Teplyakov, A. v. (2021). XPS characterization of cobalt impregnated SiO_2 and γ-Al_2O_3. *Surf. Interface Analysis* 53 (5), 475–481. doi:10.1002/sia.6935

Ci, L., Song, L., Jin, C., Jariwala, D., Wu, D., Li, Y., et al. (2010). Atomic layers of hybridized boron nitride and graphene domains. *Nat. Mater* 9 (5), 430–435. doi:10.1038/nmat2711

Díez-Ramírez, J., Sanchez, P., Kyriakou, V., Zafeiratos, S., Marnellos, G., Konsolakis, M., et al. (2017). Effect of support nature on the cobalt-catalyzed CO_2 hydrogenation. *J. CO2 Util.* 21, 562–571. doi:10.1016/j.jcou.2017.08.019

Frontera, P., Macario, A., Ferraro, M., and Antonucci, P. L. (2017). Supported catalysts for CO_2 methanation: A review. *Catalysts* 7, 59. doi:10.3390/catal7020059

Hadjiev, v. G., Iliev, M. N., and Vergilov, I. V. (1988). The Raman spectra of Co3O4. *J. Phys. C Solid State Phys.* 21 (7), L199–L201. doi:10.1088/0022-3719/21/7/007

He, F., Niu, N., Qu, F., Wei, S., Chen, Y., Gai, S., et al. (2013). Synthesis of three-dimensional reduced graphene oxide layer supported cobalt nanocrystals and their high catalytic activity in F-T CO2 hydrogenation. *Nanoscale* 5 (18), 8507–8516. doi:10.1039/c3nr03038e

Jimenez, V., Jimenez-Borja, C., Sanchez, P., Romero, A., Papaioannou, E. I., Theleritis, D., et al. (2011). Electrochemical promotion of the CO2 hydrogenation reaction on composite Ni or Ru impregnated carbon nanofiber catalyst-electrodes deposited on YSZ. *Appl. Catal. B-ENVIRONMENTAL* 107 (1–2), 210–220. doi:10.1016/j.apcatb.2011.07.016

Johnsson, F., Kjärstad, J., and Rootzén, J. (2019). The threat to climate change mitigation posed by the abundance of fossil fuels. *Clim. Policy* 19 (2), 258–274. doi:10.1080/14693062.2018.1483885

Karimi, S., Tavasoli, A., Mortazavi, Y., and Karimi, A. (2015). Cobalt supported on Graphene - a promising novel Fischer-Tropsch synthesis catalyst. *Appl. Catal. A Gen.* 499, 188–196. doi:10.1016/j.apcata.2015.04.024

Khassin, A. A. (2001). *Metal-support interactions in cobalt-aluminum co-precipitated catalysts*. XPS and CO adsorption studies'.

Krasheninnikov, A. v., Lehtinen, P. O., Foster, A. S., Pyykkö, P., and Nieminen, R. M. (2009). Embedding transition-metal atoms in graphene: Structure, bonding, and magnetism. *Phys. Rev. Lett.* 102 (12), 126807. doi:10.1103/PhysRevLett.102.126807

Kuśmierz, M. (2008). Kinetic study on carbon dioxide hydrogenation over Ru/γ-Al2O3 catalysts. *Catal. Today* 137 (2–4), 429–432. doi:10.1016/j.cattod.2008.03.003

Lahijani, P., Zainal, Z. A., Mohammadi, M., and Mohamed, A. R. (2015). Conversion of the greenhouse gas CO2 to the fuel gas CO via the boudouard reaction: A review. *Renew. Sustain. Energy Rev.* 41, 615–632. doi:10.1016/j.rser.2014.08.034

Li, Y., Qiu, W., Qin, F., Fang, H., Hadjiev, V. G., Litvinov, D., et al. (2016). Identification of cobalt oxides with Raman scattering and fourier transform infrared spectroscopy. *J. Phys. Chem. C* 120 (8), 4511–4516. doi:10.1021/acs.jpcc.5b11185

Liu, Q., Bian, B., Fan, J., and Yang, J. (2018). Cobalt doped Ni based ordered mesoporous catalysts for CO2 methanation with enhanced catalytic performance. *Int. J. Hydrogen Energy* 43 (10), 4893–4901. doi:10.1016/j.ijhydene.2018.01.132

Luo, W., Zafeiratos, S., and Zafeiratos, S. (2017). A brief review of the synthesis and catalytic applications of graphene-coated oxides. *ChemCatChem* 9 (13), 2432–2442. doi:10.1002/cctc.201700178

Mateo, D., Albero, J., and García, H. (2018). Graphene supported NiO/Ni nanoparticles as efficient photocatalyst for gas phase CO2 reduction with hydrogen. *Appl. Catal. B* 224, 563–571. doi:10.1016/j.apcatb.2017.10.071

Ojelade, O. A., and Zaman, S. F. (2021). A review on CO2hydrogenation to lower olefins: Understanding the structure-property relationships in heterogeneous catalytic systems. *J. CO2 Util.* 47, 101506. doi:10.1016/j.jcou.2021.101506

Parastaev, A., Muravev, V., Huertas Osta, E., van Hoof, A. J. F., Kimpel, T. F., Kosinov, N., et al. (2020). Boosting CO2 hydrogenation via size-dependent metal–support interactions in cobalt/ceria-based catalysts. *Nat. Catal.* 3 (6), 526–533. doi:10.1038/s41929-020-0459-4

Pham, T. H. M., Zhang, J., Li, M., Shen, T., Ko, Y., Tileli, V., et al. (2022). Enhanced electrocatalytic CO2 reduction to C_{2+} products by adjusting the local reaction environment with polymer binders. *Adv. Energy Mater* 12 (9), 2103663. doi:10.1002/aenm.202103663

Qi, Z., Chen, L., Zhang, S., Su, J., and Somorjai, G. A. (2020). A mini review of cobalt-based nanocatalyst in Fischer-Tropsch synthesis. *Appl. Catal. A Gen.* 602, 117701. doi:10.1016/j.apcata.2020.117701

Rahmati, M., Safdari, M. S., Fletcher, T. H., Argyle, M. D., and Bartholomew, C. H. (2020). Chemical and thermal sintering of supported metals with emphasis on cobalt catalysts during fischer-tropsch synthesis. *Chem. Rev.* 120 (10), 4455–4533. doi:10.1021/acs.chemrev.9b00417

Ravindra, A. v., Behera, B. C., and Padhan, P. (2014). Laser induced structural phase transformation of cobalt oxides nanostructures. *J. Nanosci. Nanotechnol.* 14 (7), 5591–5595. doi:10.1166/jnn.2014.9023

Sadasivan, S., Bellabarba, R. M., and Tooze, R. P. (2013). Size dependent reduction-oxidation-reduction behaviour of cobalt oxide nanocrystals. *Nanoscale* 5 (22), 11139–11146. doi:10.1039/c3nr02877a

ten Have, I. C., Kromwijk, J. J. G., Monai, M., Ferri, D., Sterk, E. B., Meirer, F., et al. (2022). Uncovering the reaction mechanism behind CoO as active phase for CO_2 hydrogenation. *Nat. Commun.* 13 (1), 324. doi:10.1038/s41467-022-27981-x

Torshizi, H. O., Nakhaei Pour, A., Mohammadi, A., Zamani, Y., and Kamali Shahri, S. M. (2021). Fischer-Tropsch synthesis by reduced graphene oxide nanosheets supported cobalt catalysts: Role of support and metal nanoparticle size on catalyst activity and products selectivity. *Front. Chem. Sci. Eng.* 15 (2), 299–309. doi:10.1007/s11705-020-1925-x

Tu, J., Wu, H., Qian, Q., Han, S., Chu, M., Jia, S., et al. (2021). Low temperature methanation of CO2over an amorphous cobalt-based catalyst. *Chem. Sci.* 12 (11), 3937–3943. doi:10.1039/d0sc06414a

Vogt, C., Groeneveld, E., Kamsma, G., Nachtegaal, M., Lu, L., Kiely, C. J., et al. (2018). Unravelling structure sensitivity in CO2 hydrogenation over nickel. *Nat. Catal.* 1 (2), 127–134. doi:10.1038/S41929-017-0016-Y

Wang, X., Hong, Y., Shi, H., and Szanyi, J. (2016). Kinetic modeling and transient DRIFTS–MS studies of CO2 methanation over Ru/Al2O3 catalysts. *J. Catal.* 343, 185–195. doi:10.1016/j.jcat.2016.02.001

Wigzell, F. A., and Jackson, S. D. (2017). The Genesis of supported cobalt catalysts. *Appl. Petrochem Res.* 7 (1), 9–21. doi:10.1007/s13203-016-0175-9

Xin, L., Yang, F., Rasouli, S., Qiu, Y., Uzunoglu, A., et al. (2016). Understanding Pt nanoparticle anchoring on graphene supports through surface functionalization. *ACS Catal.* 6 (4), 2642–2653. doi:10.1021/acscatal.5b02722

Zhao, K., Calizzi, M., Moioli, E., Li, M., Borsay, A., Lombardo, L., et al. (2020). Unraveling and optimizing the metal-metal oxide synergistic effect in a highly active Co (CoO)1– catalyst for CO2 hydrogenation. *J. Energy Chem.* 53, 241–250. doi:10.1016/j.jechem.2020.05.025

Zhong, L., Barreau, M., Caps, V., Papaefthimiou, V., Haevecker, M., Teschner, D., et al. (2021). Improving the catalytic performance of cobalt for CO preferential oxidation by stabilizing the active phase through vanadium promotion. *ACS Catal.* 11 (9), 5369–5385. doi:10.1021/acscatal.0c05482

Zhong, L., Barreau, M., Chen, D., Caps, V., Haevecker, M., Teschner, D., et al. (2021). Effect of manganese promotion on the activity and selectivity of cobalt catalysts for CO preferential oxidation. *Appl. Catal. B* 297, 120397. doi:10.1016/j.apcatb.2021.120397

Zhong, L., Kropp, T., Baaziz, W., Ersen, O., Teschner, D., Schlogl, R., et al. (2019). Correlation between reactivity and oxidation state of cobalt oxide catalysts for CO preferential oxidation. *ACS Catal.* 9 (9), 8325–8336. doi:10.1021/acscatal.9b02582